Spatio-temporal behavior of magnetohydrodynamic fluctuations with cross-helicity and background magnetic field

EP

R. Lugones, P. Dmitruk, P. D. Mininni (iD), A. Pouquet (iD), and W. H. Matthaeus (iD)

COLLECTIONS

EP   This paper was selected as an Editor's Pick

View Online   Export Citation   CrossMark

Spatio-temporal behavior of magnetohydrodynamic fluctuations with cross-helicity and background magnetic field 🔵EP

🌐 View Online   ⬆ Export Citation   🔴 CrossMark

R. Lugones,[1,a] P. Dmitruk,[1] P. D. Mininni,[1] 🆔 A. Pouquet,[2] 🆔 and W. H. Matthaeus[3] 🆔

AFFILIATIONS

[1]Departamento de Física, Facultad de Ciencias Exactas y Naturales, Universidad de Buenos Aires and IFIBA, CONICET, Ciudad Universitaria, 1428 Buenos Aires, Argentina

[2]Laboratory for Atmospheric and Space Physics, University of Colorado, Boulder, Colorado 80309, USA and National Center for Atmospheric Research, P.O. Box 3000, Boulder, Colorado 80307, USA

[3]Bartol Research Institute and Department of Physics and Astronomy, University of Delaware, Newark, Delaware 19716, USA

[a]Electronic mail: rlugones@df.uba.ar

ABSTRACT

We study the spatiotemporal behavior of the Elsässer variables describing magnetic and velocity field fluctuations, using direct numerical simulations of three-dimensional magnetohydrodynamic turbulence. We consider cases with relatively small, intermediate, and large values of a mean background magnetic field and with null, small, and high cross-helicity (correlations between the velocity and the magnetic field). Wavenumber-dependent time correlation functions are computed for the different simulations. From these correlation functions, the decorrelation time is computed and compared with different theoretical characteristic times: the local nonlinear time, the random-sweeping time, and the Alfvénic time. It is found that decorrelation times are dominated by sweeping effects for low values of the mean magnetic field and for low values of the cross-helicity, while for large values of the background field or of the cross-helicity and for wave vectors sufficiently aligned with the guide field, decorrelation times are controlled by Alfvénic effects. Finally, we observe counterpropagation of Alfvénic fluctuations due to reflections produced by inhomogeneities in the total magnetic field. This effect becomes more prominent in flows with large cross-helicity, strongly modifying the propagation of waves in turbulent magnetohydrodynamic flows.

I. INTRODUCTION

Turbulent fluctuations are essentially broadband, on both spatial and temporal scales, involving nonlinear couplings among a wide range of scales.[1] In incompressible magnetohydrodynamics (MHD),[2,3] these couplings are based on interactions of triads of modes,[4–8] which can be of different types, such as (local in wavenumber space) nonlinear distortions of eddies or (nonlocal in wavenumber space) sweeping of small eddies by larger ones.[9–15] Of course, these nonlinear couplings also involve interactions with waves in the flow, which are ubiquitous in MHD flows as well as in plasma turbulence.

The incompressible MHD equations sustain Alfvén waves, which in the presence of a background magnetic field $\mathbf{B}'_0$ are described by a linear dispersion relation of frequency $\omega = \mathbf{k} \cdot \mathbf{V}_A$ for the wavevector $\mathbf{k}$, with Alfvén velocity $\mathbf{V}_A = \mathbf{B}'_0/\sqrt{4\pi\rho}$ and with mass density ρ. It is well known that these waves, when considered in isolation, are also

exact solutions of the nonlinear MHD (ideal) equations. The simultaneous presence of counterpropagating fluctuations, however, activates nonlinear interactions among modes, producing dispersion, and in consequence, the waves are no longer exact solutions of the system.[16] As the background magnetic field controls the propagation velocity (i.e., the Alfvén velocity), the nonlinear interaction is influenced by the Alfvén crossing time of counterpropagating wave packets. There is therefore a competition between nonlinear interactions (i.e., turbulence) and wave propagation.[17,18]

The strength of counterpropagating fluctuations can be measured by the cross-helicity, a quantity which is a quadratic invariant of the ideal MHD equations (see Sec. II for specifics). This quantity is also of relevance for the solar wind and for space plasmas, as large-scale flows with cross-helicity (in the presence of a guide field) are often found in the interplanetary medium. A spatiotemporal analysis of field

fluctuations[14,19] can thus be performed to quantitatively study the importance of these different effects and to distinguish which is the dominant time scale among the different ones depending on the controlling parameters of the system. This kind of analysis was performed in the past for MHD flows without cross-helicity,[20–22] observing different behaviors depending on whether the turbulence is weak or strong. The prevailing conclusion, for strong turbulence, is that the time decorrelation of Fourier modes in the inertial range is typically dominated by the sweeping decorrelation due to large scale flows.[11,14,21] However, the effect of changing the strength of counterpropagating fluctuations in the spatiotemporal behavior of the flow, and in its decorrelation time, was not considered before.

In the present paper, we perform a spatiotemporal analysis of MHD turbulence, controlling simultaneously and separately the intensity of the background magnetic field and the amount of cross-helicity in the flow, extending our previous study[21] of incompressible MHD with a background magnetic field and no cross-helicity. We present several numerical solutions of the incompressible MHD equations in a turbulent steady state and analyze each time scale in the system using wavenumber-dependent time correlation functions and spatiotemporal spectra of the Elsässer variables. The spatiotemporal study of the Elsässer variables allows us to disentangle the two possible polarizations of the Alfvén waves, as well as their direction of propagation, and to quantify any imbalance between the two polarizations. We find that decorrelation times are dominated by sweeping effects for low values of the mean magnetic field and for low values of the cross-helicity, while for large values of the background field or of the cross-helicity, decorrelation times are controlled by the Alfvénic times. Moreover, for large values of the cross-helicity, we also observe counterpropagation of Alfvénic fluctuations (i.e., an inversion in the direction of propagation of one polarization of Alfvén waves), resulting from reflections in inhomogeneities of the total magnetic field produced by the turbulence. Under some conditions, this can result in the propagation of both polarizations of the Alfvén waves in the same direction. This effect strongly affects nonlinear interactions.

The structure of this paper is as follows. In Sec. II, we introduce the equations and the numerical methods employed, as well as a description of the spatiotemporal spectrum and of the correlation functions. Results are presented in Sec. III. Finally, discussions and conclusions are presented in Sec. IV.

II. EQUATIONS AND NUMERICAL SIMULATIONS
A. The MHD equations and the Elsässer fields

The incompressible MHD equations (momentum and induction equations) in dimensionless units as solved in the numerical simulations are

$$\frac{\partial \mathbf{v}}{\partial t} + \mathbf{v} \cdot \nabla \mathbf{v} = -\frac{1}{\rho}\nabla p + \mathbf{j} \times \mathbf{B} + \frac{1}{R}\nabla^2 \mathbf{v} + \mathbf{F}_v, \tag{1}$$

$$\frac{\partial \mathbf{b}}{\partial t} = \nabla \times (\mathbf{v} \times \mathbf{B}) + \frac{1}{R_m}\nabla^2 \mathbf{b} + \mathbf{F}_b, \tag{2}$$

where $\mathbf{v}$ is the plasma bulk velocity, $\mathbf{B} = \mathbf{b} + \mathbf{B}_0$ is the total magnetic field (in units of an Alfvénic speed, and obtained from the total magnetic field $\mathbf{B}'$ in Gaussian units after dividing by $\sqrt{4\pi\rho}$, where ρ is the plasma density), and $\mathbf{F}_v$ and $\mathbf{F}_b$ are forcing terms to be discussed in more detail below. The total magnetic field has a fluctuating part $\mathbf{b}$,

and a mean DC field $\mathbf{B}_0 = B_0\hat{\mathbf{x}}$. Finally, $\mathbf{j} = \nabla \times \mathbf{b}$ is the current density and p is the plasma pressure. The units are based on a characteristic speed v_0, which for MHD is chosen to be the typical Alfvén speed of the magnetic field fluctuations, $v_0 = \sqrt{\langle b^2 \rangle /(4\pi\rho)}$, where $\langle . \rangle$ denotes a spatial average. The dimensionless parameters appearing in the equations are the kinetic and magnetic Reynolds numbers, $R = v_0 L/\nu$ and $R_m = v_0 L/\mu$, respectively, with ν the kinematic viscosity, μ the magnetic diffusivity, and L the characteristic length scale (the simulation box side length is defined as $2\pi L$). The unit time is $t_0 = L/v_0$, which for MHD becomes the Alfvén crossing time based on magnetic field fluctuations. The Elsässer fields are then defined as

$$\mathbf{z}^{\pm} = \mathbf{v} \pm \mathbf{b}. \tag{3}$$

In terms of the Elsässer fields, the MHD equations can be written[14] as

$$\partial_t \mathbf{z}^{\pm} = \pm \mathbf{V}_{\mathrm{A}} \cdot \nabla \mathbf{z}^{\pm} - \mathbf{z}^{\mp} \cdot \nabla \mathbf{z}^{\pm} - \nabla P + \frac{1}{R}\nabla^2 \mathbf{z}^{\pm}, \tag{4}$$

with P the total pressure divided by the plasma density, and with the assumption that $R = R_m$. In the rhs of Eq. (4), we explicitly separated the convective term into a linear part describing Alfvénic propagation with $\mathbf{V}_{\mathrm{A}} = \mathbf{B}_0$ the Alfvén velocity based on the background magnetic field (with $\mathbf{B}_0$ the field in units of velocity), and the nonlinear part describing the interaction among counterpropagating wavelike fluctuations. It is evident from these equations that both Elsässer fields must be present to activate the nonlinear interactions.

The ideal invariants (i.e., with zero viscosity and resistivity) of incompressible MHD theory can be written in terms of the Elsässer fields. The total energy E (kinetic plus magnetic) in terms of these variables is

$$E = \frac{1}{2}\int \left(|\mathbf{v}|^2 + |\mathbf{b}|^2\right) dV = \frac{1}{4}\int \left(|\mathbf{z}^+|^2 + |\mathbf{z}^-|^2\right) dV, \tag{5}$$

while the cross-helicity H_c is

$$H_c = \int \mathbf{v} \cdot \mathbf{b}\, dV = \frac{1}{4}\int \left(|\mathbf{z}^+|^2 - |\mathbf{z}^-|^2\right) dV. \tag{6}$$

The ratio $\sigma_c = H_c/E$ measures the amount of counterpropagating fluctuations in the system. A value $\sigma_c = \pm 1$ corresponds to only one type of fluctuations $\mathbf{z}^{\pm}$, while $\sigma_c = 0$ represents equipartition between both fields.

As later in the analysis we will be interested in the effect of flow inhomogeneities in the propagation of these fluctuations, following the works of Matthaeus et al.[23] and Zhou and Matthaeus,[24] we can linearize the ideal MHD equations considering the presence of an inhomogeneous background magnetic field and/or an inhomogeneous background flow. From these works, the general MHD equations (including density fluctuations) can be written as

$$\partial_t \mathbf{z}^{\pm} + \left(L_{\mathbf{x}}^{\pm} + L^{\pm}\right)\mathbf{z}^{\pm} + M_{ik}^{\pm}\mathbf{z}_k^{\mp} = 0. \tag{7}$$

The linear operators $L_{\mathbf{x}}^{\pm}$, $L^{\pm}$, and $M_{ik}^{\pm}$ involve gradients acting on both the large- and the small-scale fields and are given by

$$L_{\mathbf{x}}^{\pm} = (\mathbf{U} \mp \mathbf{V}_{\mathrm{A}}) \cdot \nabla, \tag{8}$$

$$L^{\pm} = \frac{1}{2}\nabla \cdot \left(\frac{\mathbf{U}}{2} \pm \mathbf{V}_{\mathrm{A}}\right), \tag{9}$$

and

$$M_{ik}^{\pm} = \nabla_k U_i \pm \frac{1}{\sqrt{4\pi\rho}} \nabla_k B_i' - \frac{1}{2}\delta_{ik}\nabla \cdot \left(\frac{\mathbf{U}}{2} \pm \mathbf{V}_A\right), \quad (10)$$

where $\mathbf{U}$ is a background flow. Here, both $\mathbf{U}$ and $\mathbf{V}_A$ can include large-scale inhomogeneities (including, for $\mathbf{V}_A$, inhomogeneities associated with density fluctuations). The mixing terms (those involving the $M_{ik}^{\pm}$ operators) allow the possibility of creating counter propagating fluctuations out of a single-sign propagating fluctuation, by means of reflections due to inhomogeneities in any of the background fields.[25] In this sense, even if the system starts from an initial condition with only one sign of propagating fluctuations, the reflections by inhomogeneous background fields will create an amount of counter propagating fluctuations which will turn on nonlinearities, producing dispersion and turbulence.[26,27] But this effect can also result, in flows with both polarizations of Alfvénic excitations, in the counterpropagation of one of the excitations, as will be shown from numerical data in Sec. III.

B. Wavenumber-frequency spectrum and correlation functions

Using scaling arguments, different characteristic times in the system can be estimated. The local eddy turnover time or isotropic non-linear time scale can be defined as $\tau_{nl} \sim 1/[kv(k)]$, where $v(k)$ is the amplitude of the velocity fluctuations at scale $\sim 1/k$. Considering a Kolmogorov-like scaling $v(k) \sim v_{rms}(kL)^{-1/3}$, the nonlinear time in the inertial range can be written as

$$\tau_{nl} = C_{nl}\left[v_{rms}L^{-1/3}\left(\sqrt{k_{\perp}^2 + k_{\parallel}^2}\right)^{2/3}\right]^{-1}, \quad (11)$$

where C_{nl} is a dimensionless constant of order one, and $k_{\parallel}$ and $k_{\perp}$ denote the wavenumbers parallel and perpendicular to the background magnetic field. Here, $v_{rms} = \langle|\mathbf{v}|^2\rangle^{1/2}$ is a global quantity, dominated by contributions from the large scales.[3,28]

Another time decorrelation effect is governed by the sweeping characteristic time, which at the scale $\sim 1/k$ can be expressed as

$$\tau_{sw} = C_{sw}\left(v_{rms}\sqrt{k_{\perp}^2 + k_{\parallel}^2}\right)^{-1}. \quad (12)$$

This time corresponds to the advection of small-scale structures by the large-scale flow. Finally, a characteristic Alfvén time can be defined as

$$\tau_A = C_A\left(v_A k_{\parallel}\right)^{-1}. \quad (13)$$

In the last two expressions, C_{sw} and C_A also are dimensionless constants of order unity.

These are not all the time scales that could be present in MHD turbulence, but the ones most relevant for the discussions in the following section (Sec. III). As an example, another time scale worth mentioning is the decorrelation time of triple moments when there is no equipartition between magnetic and kinetic energies, e.g., in the dynamo context.[29]

To disentangle these time scales in the flow, and to identify which is the most relevant time scale at a given spatial scale, two tools can be used: the statistical properties of the correlation function in space and time, and the wavenumber-frequency spectrum. We start by

introducing the former. The statistics of the Elsässer fields can be characterized by the spatiotemporal two-point autocorrelation function,[14]

$$R^{\pm}(\mathbf{r}, \tau) = \langle\mathbf{z}^{\pm}(\mathbf{x}, t) \cdot \mathbf{z}^{\pm}(\mathbf{x} + \mathbf{r}, t + \tau)\rangle/\langle|\mathbf{z}^{\pm}|^2\rangle. \quad (14)$$

The Fourier transform in $\mathbf{r}$ leads to a time-lagged spectral density which can be further factorized as $S(\mathbf{k}, \tau) = S(\mathbf{k})\Gamma(\mathbf{k}, \tau)$. The function $\Gamma(\mathbf{k}, \tau)$ is the scale-dependent correlation function[30–32] which describes the time decorrelation of each spatial mode $\mathbf{k}$, that is, the loss of memory of fluctuations with characteristics lengths of order k_x^{-1}, k_y^{-1}, and k_z^{-1}.

When there is a preferential direction in the flow (as in the present case of MHD turbulence with a guide magnetic field), it is useful to assume axial symmetry in Fourier space and to write $\Gamma(\mathbf{k}, \tau) = \Gamma(k_{\perp}, k_{\parallel}, \tau)$. As this function is three dimensional, it is also useful to study $\Gamma(k_{\perp}, k_{\parallel}, \tau)$ with one of the arguments fixed; for instance, fixing a value of $k_{\perp}$ and analyzing $\Gamma(k_{\perp}, k_{\parallel}, \tau)$ as a function of $k_{\parallel}$ and τ gives us information on fluctuations that vary only in the parallel direction, and allow us to distinguish between decorrelation arising from Alfvénic nonlinear interactions or sweeping.

The Fourier transform in the time lag of the scale-dependent correlation function results in the wavenumber-frequency spectrum $E^{\pm}(\mathbf{k}, \omega)$ for each of the Elsässer fields. This property follows directly from 1 that states that the Fourier transform of a signal autocorrelation is the power spectrum of the same signal (see Refs. 19 and 33, and pp. 35–36 from Ref. 34 for further details). The spectra $E^{\pm}(\mathbf{k}, \omega)$ allow identification of modes satisfying a generalized dispersion relation of the system, and provide a direct measurement of how much energy is in those modes, and of how much energy is in other modes. For the two separate Elsässer fields, from Eqs. (5) and (6) it is easy to see that

$$E = E^+ + E^-, \quad H_c = E^+ - E^-, \quad (15)$$

where $E^{\pm} = \int |\mathbf{z}^{\pm}|^2/4 \, dV$. Thus, for the wavenumber-frequency spectra of the Elsässer fields, the two following relations hold,

$$E^+(\mathbf{k}, \omega) = [E(\mathbf{k}, \omega) + H_c(\mathbf{k}, \omega)]/2, \quad (16)$$

$$E^-(\mathbf{k}, \omega) = [E(\mathbf{k}, \omega) - H_c(\mathbf{k}, \omega)]/2. \quad (17)$$

Therefore, computation of the wavenumber-frequency spectra of the energy and of the cross-helicity allows unique determination of the wavenumber-frequency spectra of the Elsässer fields, and vice versa.

C. Numerical simulations

To solve numerically the incompressible MHD Eqs. (1) and (2), we employ a parallel pseudospectral code.[35–37] We consider a spatial resolution of $N^3 = 512^3$ grid points, with a second-order Runge-Kutta time integration scheme. Spatial resolution is moderate as we need to store a large amount of data in space and time to compute the correlation functions and spectra defined in Sec. II B. Values considered for the intensity of the external magnetic field are $B_0 = 0$, 0.25, 1, 2, 4, and 8 (in units of the initial rms magnetic fluctuations value). We assume periodic boundary conditions in a cube of side $2\pi L$ (with L the initial correlation length of the fluctuations, defined as the unit length). Aliasing is removed by the two-thirds rule truncation method.

The initial condition in all simulations consists of nonzero amplitudes for the $\mathbf{v}(\mathbf{k})$ and $\mathbf{b}(\mathbf{k})$ fields, equipartitioned in all the wavenumbers within shells $1.1 \leq k \leq 4$ (in units of $2\pi L/\lambda$, with λ the

wavelength). Random phases are chosen for all Fourier modes in both fields. To keep the system in a turbulent steady state, we apply a driving consisting of forcing terms $\mathbf{F}_b$ and $\mathbf{F}_v$ for $\mathbf{b}$ and $\mathbf{v}$, respectively, in Eqs. (1) and (2). $\mathbf{F}_b$ and $\mathbf{F}_v$ are bands limited to a fixed set of Fourier modes in the band $0.9 \leq k \leq 1.8$. The driving has a random and a time-coherent component, and the correlation time of the forcing is $\tau_f \approx 1$ (of the order of the unit time t_0), which is larger than all the characteristic times defined in the Sec. II B. To change the level of cross-helicity in the flow, correlations were introduced between the mechanical and electromotive drivings, resulting at late times (depending on the level of cross correlation between the drivers) in a normalized cross-helicity of $\sigma_c = 0$, 0.3, or 0.9 (these values correspond to the time average in the turbulent steady state; in practice, in each simulation, the instantaneous cross-helicity fluctuates in time around the reported mean values).

Note the different values of B_0 and of σ_c explored result in a total of 18 simulations (see Table I). All simulations were continued until the system reached a turbulent steady state, and then continued further to perform the spatiotemporal analysis on the evolution of the Elsässer fields presented in the Sec. III. We will first characterize the spatial behavior of the flows (in particular considering the degree of anisotropy as the intensity of the background flow is increased), to then study the behavior of the Elsässer fluctuations using the spatiotemporal information.

III. RESULTS

A. Wavenumber spectra

After the system reached the turbulent steady state, we analyzed the results during 10 large-scale unit times, after verifying that this time span was enough to ensure convergence of spatiotemporal spectra and correlation functions.

We start discussing the spatial spectral, to characterize the turbulence and to quantify its anisotropy as the intensity of the guide field is varied, for different values of the cross-helicity. But first we need to define some quantities, as we are dealing with anisotropic flows. In principle, we could study spectra in terms of the wave vector $\mathbf{k}$, but this results in a three-dimensional spectral density. Using the preferential direction associated with the guide field, reduced spectra can be defined that simplify substantially the data analysis.

The axisymmetric energy spectrum $e(k_\perp, k_\parallel, t)$ provides information on the anisotropy of the turbulence relative to the guide field.[38] It is defined as

$$
e(k_\perp, k_\parallel, t) = \sum_{\substack{k_\perp \leq |\mathbf{k} \times \hat{x}| < k_\perp + 1 \\ k_\parallel \leq k_x < k_\parallel + 1}} |\hat{u}(\mathbf{k}, t)|^2 + |\hat{b}(\mathbf{k}, t)|^2
$$
$$
= \int \left(|\hat{u}(\mathbf{k}, t)|^2 + |\hat{b}(\mathbf{k}, t)|^2 \right) |\mathbf{k}| \sin \theta_k \, d\phi_k. \quad (18)
$$

The first equality corresponds to the way the spectra are computed in the simulations (as Fourier modes are discrete), while the second corresponds to the theoretical definition in the continuum case. Since the guide field is $\mathbf{B}_0 = B_0 \hat{x}$, in both cases, the wave vector components $k_\parallel = k_x$ and $k_\perp = \sqrt{k_y^2 + k_z^2}$, and the polar angles in Fourier space θ_k and ϕ_k are relative to the x-axis. That is, in Eq. (18), $\theta_k = \arctan(k_\perp / k_\parallel)$ is the colatitude in Fourier space with respect to the x-axis, and ϕ_k is the longitude with respect to the y-axis. Note that below we treat the discrete and continuum expressions of Fourier spectra as equivalent, bearing in mind that in all cases integrals should be replaced by sums when required for the numerics.

Using the axisymmetric spectrum, one can define the time averaged isotropic energy spectrum $E(k)$ as
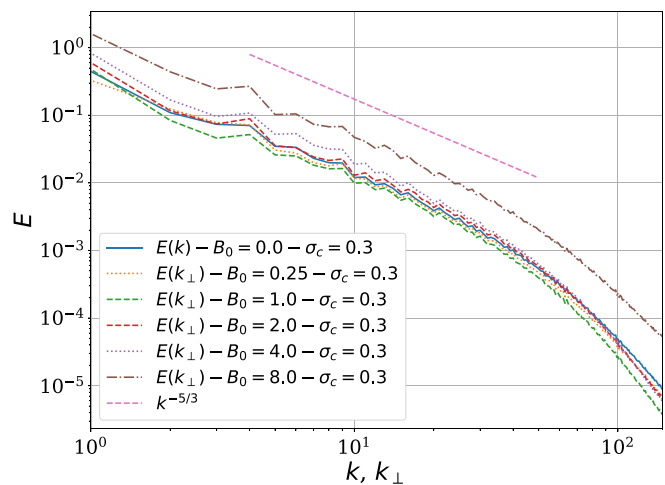
$$
E(k) = \frac{1}{T} \int \int e(|\mathbf{k}_\perp|, k_\parallel, t) |\mathbf{k}| \, d\theta_k \, dt, \quad (19)
$$

and the reduced perpendicular energy spectrum $E(k_\perp)$[38] as

$$
E(k_\perp) = \frac{1}{T} \int \int e(|\mathbf{k}_\perp|, k_\parallel, t) \, dk_\parallel \, dt, \quad (20)
$$

where in the latter case, we integrate over parallel wave numbers to obtain a spectrum that depends only on $k_\perp$, and in both cases, we average in time over a (sufficiently long) time T.

The reduced perpendicular energy spectra $E(k_\perp)$ are shown in Fig. 1 for the simulations with $B_0 = 0.25$, 1, 2, 4, and 8 with normalized cross-helicity $\sigma_c = 0.3$. In this figure, we also show the isotropic energy spectrum $E(k)$ for the simulation with $B_0 = 0$, with $\sigma_c = 0.3$. The simulations with $\sigma_c = 0$ and $\sigma_c = 0.9$ display a similar behavior. A Kolmogorov power law is also indicated in the figure as reference. As can be seen, despite the moderate spatial resolution of the runs, the observed spatial spectra are compatible with Kolmogorov scaling $\sim k_\perp^{-5/3}$, and the simulations are well resolved displaying a dissipative range for large wavenumbers (for example, the Kolmogorov

TABLE I. List of numerical simulations performed, with guide field $\mathbf{B} = B_0 \hat{x}$ and normalized cross-helicity σ_c.

	$B_0 = 0$	$B_0 = 0.25$	$B_0 = 1$	$B_0 = 2$	$B_0 = 4$	$B_0 = 8$
	0	0	0	0	0	0
$\sigma_c \approx$	0.3	0.3	0.3	0.3	0.3	0.3
	0.9	0.9	0.9	0.9	0.9	0.9

FIG. 1. Reduced perpendicular energy spectra $E(k_\perp)$ for simulations with $B_0 = 0$, 0.25, 1, 2, 4, and 8. All curves correspond to the case $\sigma_c = 0.3$, but the cases with $\sigma_c = 0$ and 0.9 show the same behavior. Kolmogorov scaling, $\sim k_\perp^{-5/3}$, is shown as the reference.

dissipation wavenumbers k_ν are $k_\nu \approx 91, 152$, and 122 for the simulations with $B_0 = 1$ and $\sigma_c = 0, 0.3$, and 0.9, respectively).

We can see the spectral behavior (and of the anisotropy of the flows) in more detail in Fig. 2. There, we show isocontours of the axisymmetric energy spectrum $e(k_\perp, k_\parallel)$ (i.e., the energy density as a function of perpendicular and parallel wavenumbers) for $B_0 = 0, 1, 4$, and 8, and in all cases for flows with $\sigma_c = 0.3$. As a reference, we also indicate the curves (in Fourier space) where the Alfvén time is equal to either the sweeping time, or the nonlinear time. In other words, these curves separate regions in which (from theoretical arguments) the fastest time scale can be expected to be either τ_A (above the dashed red curve) or τ_{nl} (below the solid blue curve). The sweeping time can be relevant for all modes below the dashed red curve.

Note that for $B_0 \neq 0$ the energy is not distributed isotropically in the axisymmetric spectra in Fig. 2. Energy tends to accumulate in modes with small $k_\parallel$ as B_0 is increased, and for $B_0 = 4$ and 8, a

substantial fraction of the energy accumulates in the vicinity of the curves satisfying $\tau_A \approx \tau_{sw}$ and $\tau_A \approx \tau_{nl}$.

B. Wavenumber-frequency spectra

We calculate the energy spectrum $E(\mathbf{k}, \omega)$ from the relation

$$E(\mathbf{k}, \omega) = \frac{1}{2}|\hat{u}(\mathbf{k}, \omega)|^2 + \frac{1}{2}|\hat{b}(\mathbf{k}, \omega)|^2, \tag{21}$$

where $\hat{u}(\mathbf{k}, \omega)$ and $\hat{b}(\mathbf{k}, \omega)$ are the Fourier transforms in time and in space of the velocity and the magnetic fields, respectively. The main results of the present study are summarized in Figs. 3–6, which quantify the spatiotemporal behavior of the Elsässer fields separately. These figures show the normalized wavevector and frequency spectra of the $\mathbf{z}^+$ and $\mathbf{z}^-$ variables, for simulations with different values of the background mean field B_0 and normalized cross-helicity σ_c. As the spectra are multidimensional, in all cases we show slices of the spectrum for
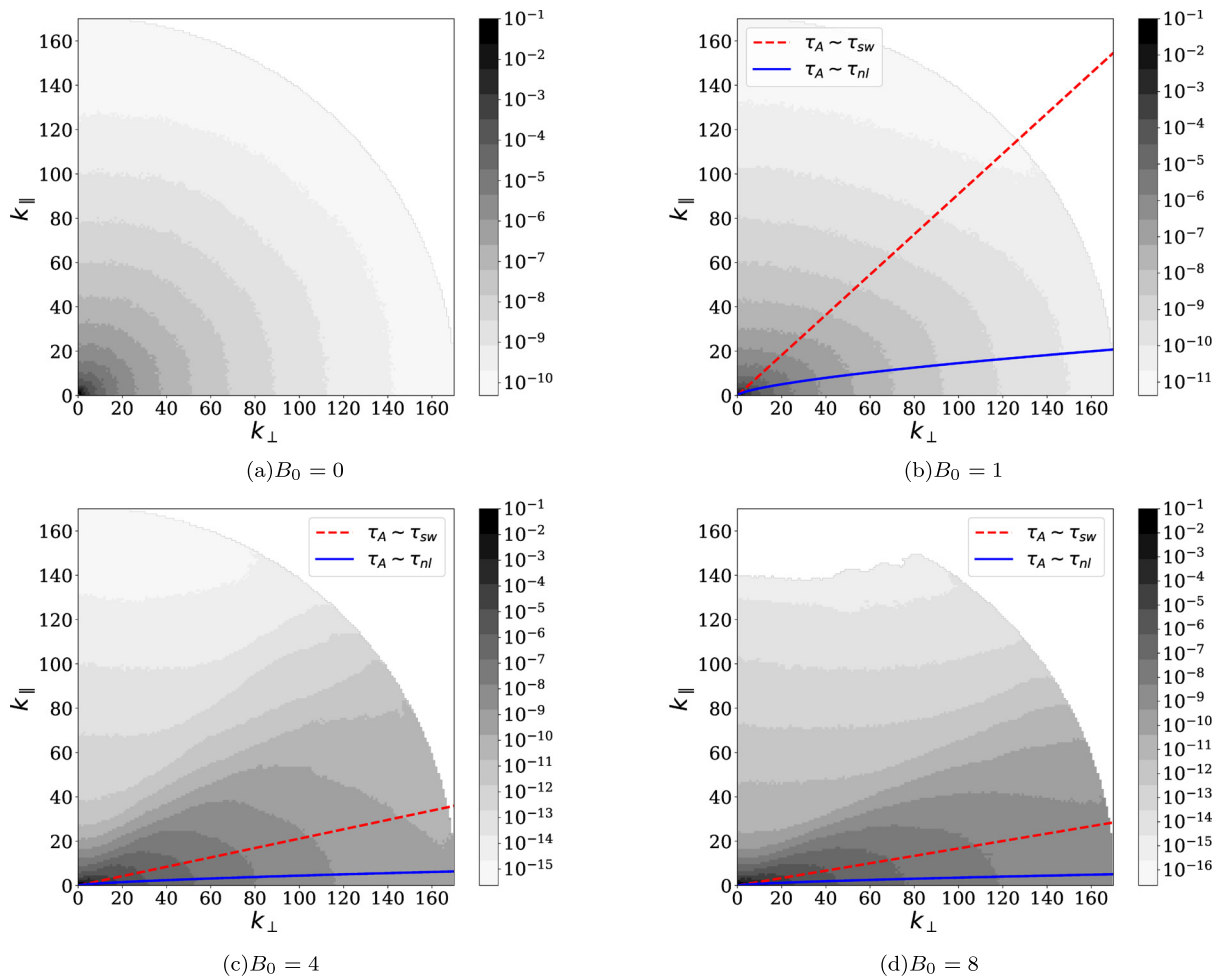
FIG. 2. Isocontours of the axisymmetric energy spectrum $e(k_\perp, k_\parallel)$ for $B_0 = 0, 1, 4$, and 8, and for $\sigma_c = 0.3$. In all cases, dark means larger energy density (in logarithmic scale). The lines indicate the modes for which the sweeping time (red dashed line) or the local nonlinear time (solid blue line) becomes equal to the Alfvén time. For large B_0, the flow becomes more anisotropic, and isocontours change shape as they cross these lines. Note also the increase in the energy in modes that have the Alfvén time as the fastest time (i.e., of modes below the solid blue curve) as B_0 increases.
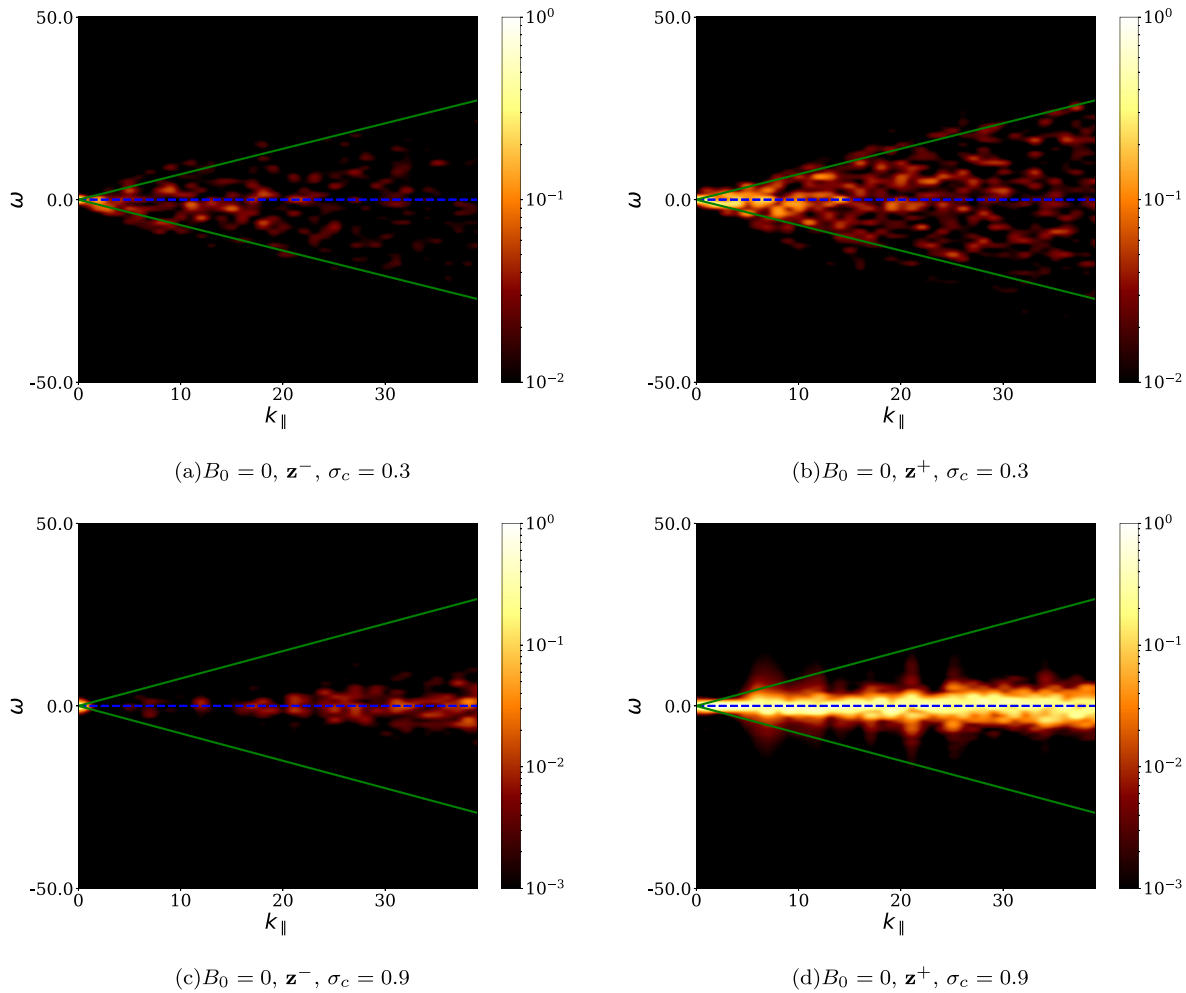
FIG. 3. Normalized wave vector and frequency spectra $E^{\pm}(\mathbf{k}, \omega)/E^{+}(\mathbf{k})$ of $\mathbf{z}^-$ (left) and $\mathbf{z}^+$ (right), for the isotropic simulations ($B_0 = 0$) with $\sigma_c = 0.3$ [top, panels (a) and (b)] and $\sigma_c = 0.9$ [bottom, panels (c) and (d)], as a function of $k_{\parallel}$ and for fixed $k_{\perp} = 0$. Lighter regions indicate larger energy density. The spectra correspond to the power in the time and space Fourier transform of the fields, such that accumulation of energy in modes near the dispersion relation (or in all modes below the sweeping curve) points to a dominance of a physical effect (i.e., of its associated frequency) in the dynamics of a given scale $\sim 1/k_{\parallel}$. As a reference, the sweeping time relation giving by Eq. (12) is indicated by solid (green) lines. A broad excitation of modes is observed for all modes with $\omega \leq 1/\tau_{sw}$ (sweeping) in panels (a) and (b), and for $\omega \approx 0$ in panels (c) and (d).
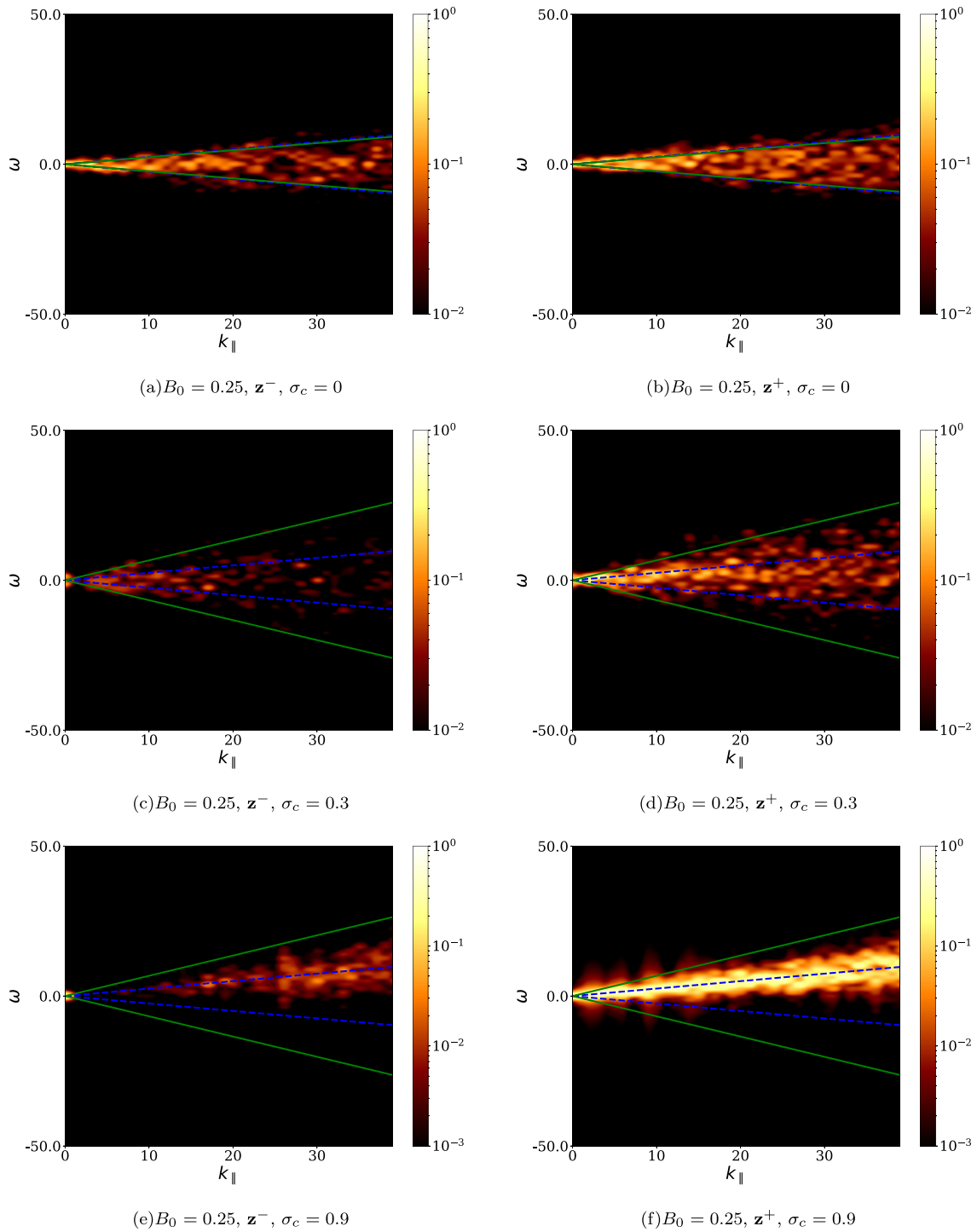
$k_{\perp} = 0$ and as a function of $k_{\parallel}$ and ω (other slices, with other values of $k_{\perp}$, display the same behavior for the waves reported below).

Figure 3 shows these spatiotemporal spectra for simulations with $B_0 = 0$. In this case, the dispersion relation for Alfvénic fluctuations becomes $\omega = 0$, and Alfvén waves are indistinguishable (in this spectrum) from slow modes such as turbulent eddies. The sweeping relation, for eddies with velocity v_{rms}, becomes $\omega = \pm v_{rms}k$, and in practice, as all turbulent eddies with this velocity (or a smaller velocity) can randomly sweep small-scale structures in the flow, the relation for random sweeping becomes $|\omega| \leq v_{rms}k$. Both relations are indicated, respectively, by dashed and solid lines in Fig. 3.

Accumulation of energy in the spectra in Fig. 3 can be seen for all modes in the region enclosed by the sweeping relation, evidencing the presence of broadband (strong) turbulence rather than of wave turbulence or linear wave propagation. Moreover, for large values of the normalized cross-helicity ($\sigma_c = 0.9$), energy accumulates instead in

modes with $\omega \approx 0$, and more energy can be observed in $\mathbf{z}^+$ modes when compared to the $\mathbf{z}^-$ modes. From these spectra, we can conclude that for $B_0 = 0$ and $\sigma_c = 0$ the dominant time scale is that of the sweeping, while for large values of σ_c either the nonlinear time scale or the Alfvén time become dominant.

Figure 4 shows the spatiotemporal spectra for simulations with $B_0 = 0.25$. The case with $\sigma_c = 0$ shows again a broad range of fluctuations in the range of frequencies enclosed by the sweeping relation. As the value of σ_c is increased, the $\mathbf{z}^+$ fluctuations become dominant, a situation which is more evident in the case with $\sigma_c = 0.9$. Also, as σ_c is increased, energy in $\mathbf{z}^+$ fluctuations leaves the funnel defined by the sweeping relation, and concentrates in the vicinity of the dispersion relation of Alfvén waves $\omega^+ = +\mathbf{V}_A \cdot \mathbf{k}$ (see the case with $\sigma_c = 0.9$ in Fig. 4). Note that the choice of signs for waves described by $\mathbf{z}^{\pm} = \mathbf{z}_0^{\pm} e^{i(\mathbf{k} \cdot \mathbf{x} + \omega^{\pm} t)}$ follows from the fact that the Fourier transforms used in space and in time follow the same sign convention, and where $\mathbf{z}_0^{\pm}$

(a)$B_0 = 0.25$, $\mathbf{z}^-$, $\sigma_c = 0$

(b)$B_0 = 0.25$, $\mathbf{z}^+$, $\sigma_c = 0$

(c)$B_0 = 0.25$, $\mathbf{z}^-$, $\sigma_c = 0.3$

(d)$B_0 = 0.25$, $\mathbf{z}^+$, $\sigma_c = 0.3$

(e)$B_0 = 0.25$, $\mathbf{z}^-$, $\sigma_c = 0.9$

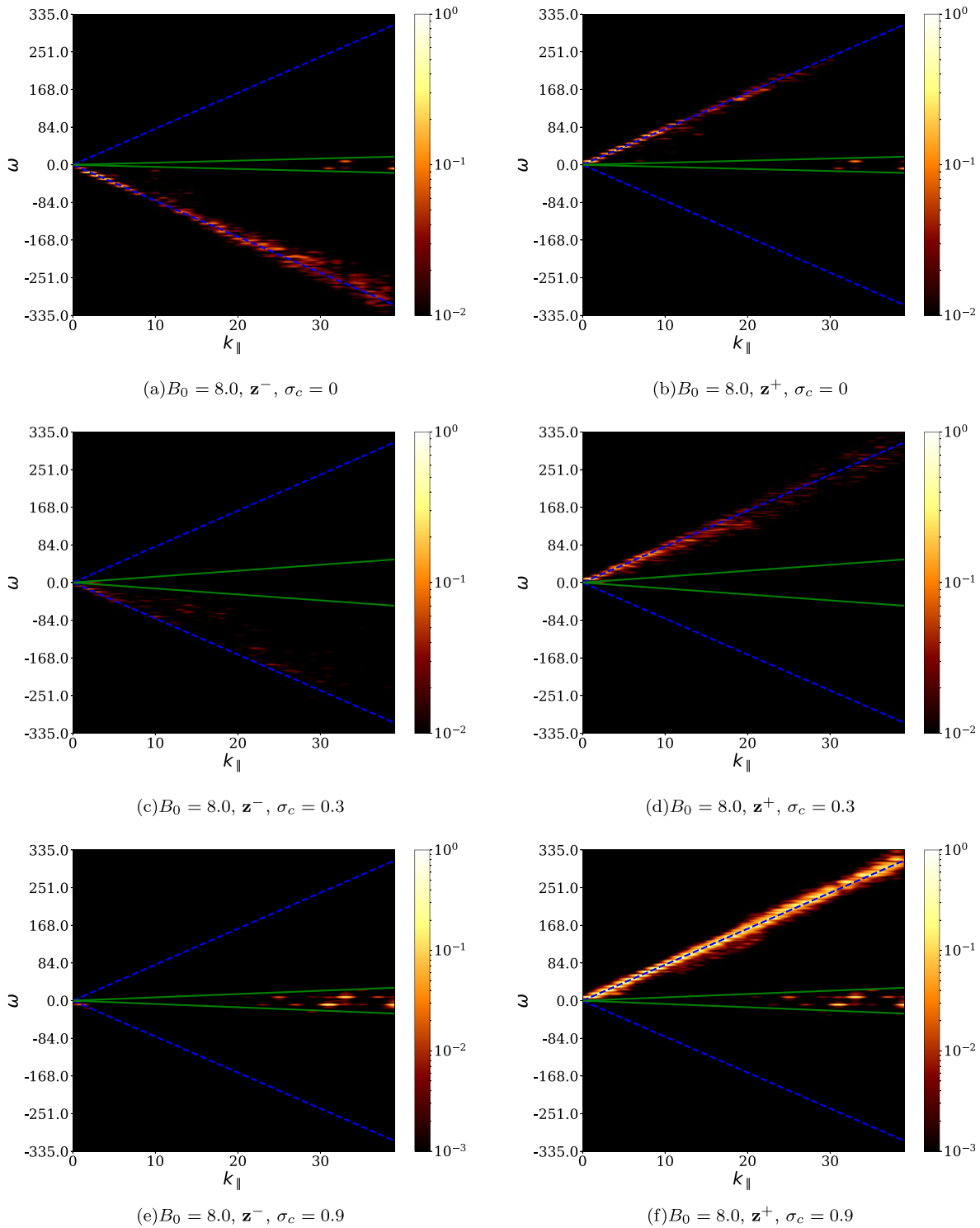(f)$B_0 = 0.25$, $\mathbf{z}^+$, $\sigma_c = 0.9$

FIG. 4. Normalized spectra $E^{\pm}(\mathbf{k}, \omega)/E^+(\mathbf{k})$ of $\mathbf{z}^-$ (left) and $\mathbf{z}^+$ (right), for the runs with $B_0 = 0.25$, for modes with $k_\perp = 0$, and thus as a function of $k_\parallel$ and ω. Panels (a) and (b) correspond to $\sigma_c = 0$, (c) and (d) to $\sigma_c = 0.3$, and (e) and (f) to $\sigma_c = 0.9$. The sweeping time relation, given by Eq. (12), is indicated by solid (green) lines, and the dashed (blue) lines indicate the dispersion relation of Alfvén waves. Lighter regions indicate larger energy density, and the accumulation of energy in modes near the dispersion relation (or in all modes below the sweeping curve) points to a dominance of a physical effect (i.e., of its associated frequency) in the dynamics of a given scale $\sim 1/k_\parallel$. For low normalized cross-helicity, σ_c sweeping is the dominant effect, while for large σ_c, energy accumulates near the dispersion relation of the waves, albeit for both $\mathbf{z}^+$ and $\mathbf{z}^-$ with the same sign of the frequency ω.
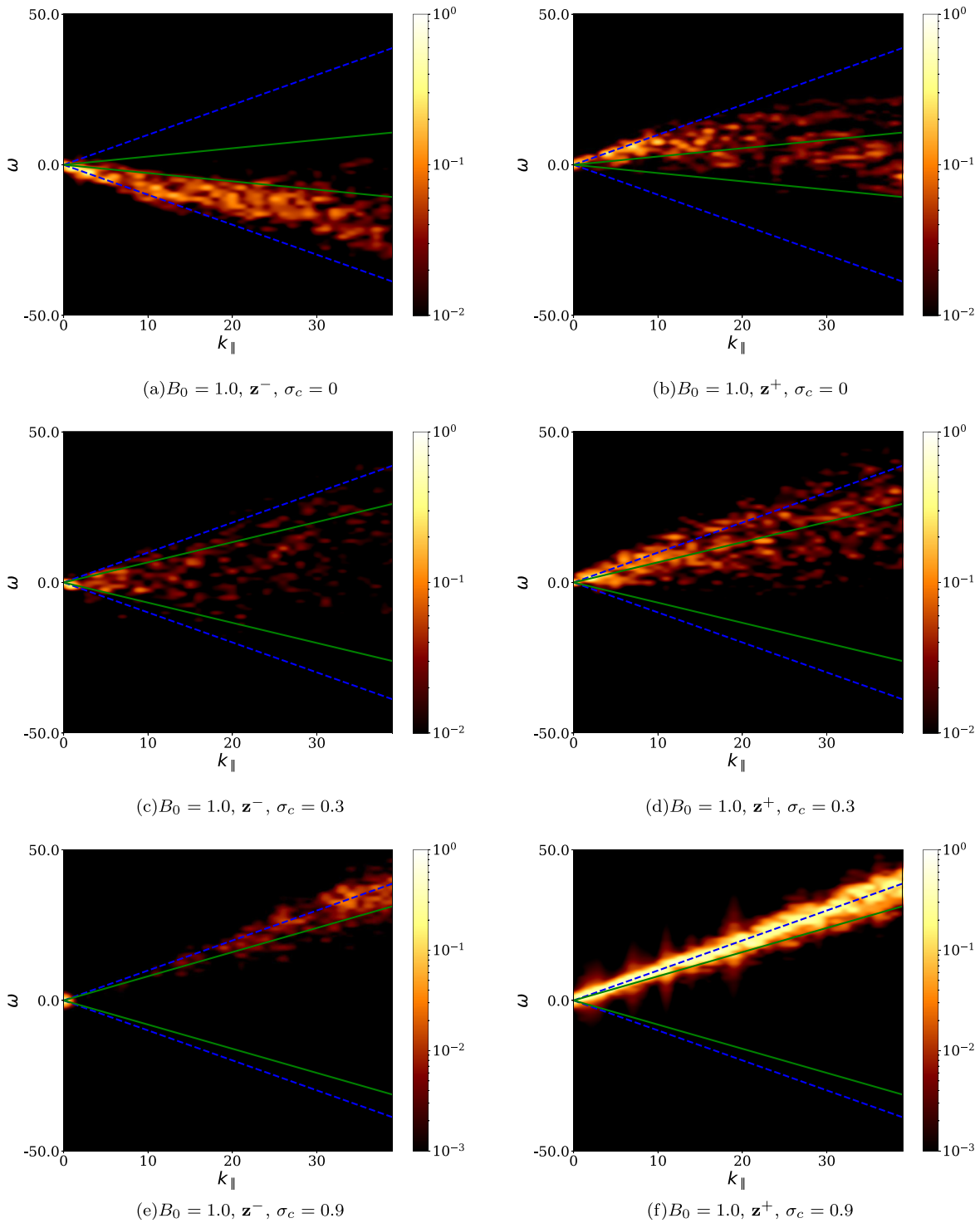
FIG. 5. Normalized spectra $E^{\pm}(\mathbf{k}, \omega)/E^{+}(\mathbf{k})$ of $\mathbf{z}^{-}$ (left) and $\mathbf{z}^{+}$ (right), for the runs with $B_0 = 1$, for modes with $k_{\perp} = 0$, and thus as a function of $k_{\parallel}$ and ω. Panels (a) and (b) correspond to $\sigma_c = 0$, (c) and (d) to $\sigma_c = 0.3$, and (e) and (f) to $\sigma_c = 0.9$. The sweeping time relation, given by Eq. (12), is indicated by solid (green) lines, and the dashed (blue) lines indicate the dispersion relation of Alfvén waves. Lighter regions indicate larger energy density. In this case, power for $\sigma_c = 0$ is concentrated in a region near the wave dispersion relations $\omega^{\pm} \approx \pm \mathbf{V}_A \cdot \mathbf{k}$ up to $k_{\parallel} \approx 10$. For $\sigma_c = 0.9$, both fields $\mathbf{z}^{+}$ and $\mathbf{z}^{-}$ follow the same dispersion relation $\omega \approx +\mathbf{V}_A \cdot \mathbf{k}$, and Alfvénic excitations dominate over all scales.

FIG. 6. Normalized spectra $E^{\pm}(\mathbf{k}, \omega)/E^{+}(\mathbf{k})$ of $\mathbf{z}^{-}$ (left) and $\mathbf{z}^{+}$ (right), for the runs with $B_0 = 8$, for modes with $k_{\perp} = 0$, and thus as a function of $k_{\parallel}$ and ω. Panels (a) and (b) correspond to $\sigma_c = 0$, (c) and (d) to $\sigma_c = 0.3$, and (e) and (f) to $\sigma_c = 0.9$. The sweeping time relation, given by Eq. (12), is indicated by solid (green) lines, and the dashed (blue) lines indicate the dispersion relation of Alfvén waves. Lighter regions indicate larger energy density. In all cases, power is concentrated in a narrow region near the wave dispersion relations $\omega^{\pm} \approx \pm \mathbf{V}_{\mathrm{A}} \cdot \mathbf{k}$ or near $\omega \approx 0$, for all the wavenumbers studied, and there is no evidence of counterpropagation of waves.

are the amplitudes of the waves. This way, the sign of ω^+ implies that $\mathbf{z}^+$ fluctuations propagate antiparallel to the guide field, as expected. However, in an apparent contradiction, the waves with the opposite polarization, i.e., the $\mathbf{z}^-$ fluctuations, also populate (albeit with smaller amplitude) the same upper branch of the Alfvénic wave dispersion relation. As the $\mathbf{z}^-$ fluctuations satisfy another dispersion relation ($\omega^- = -\mathbf{V}_A \cdot \mathbf{k}$), in the linear regime these fluctuations should populate instead the lower branch of the dispersion relation shown in Fig. 4. This behavior indicates that $\mathbf{z}^-$ fluctuations also propagate in real space in the direction antiparallel to the guide field (i.e., with negative velocity), instead of parallel to this field (i.e., with positive velocity) as would be expected. Such a behavior was predicted by Hollweg[39] for the solar wind and caused by, e.g., reflections of waves in density fluctuations in the interplanetary medium, using a WKB expansion. In our case, the flow is incompressible and density is uniform in space and constant in time.

As B_0 is increased, this effect becomes more evident. In Fig. 5, we show the spatiotemporal spectra for simulations with $B_0 = 1$. Now energy tends to concentrate near the dispersion relation of the Alfvén waves for all values of σ_c, i.e., as we increase the value of B_0 the relevance of random sweeping decreases and Alfvén waves become more important. For $\sigma_c = 0$, we observe waves propagating in both directions: $\mathbf{z}^+$ fluctuations propagate antiparallel to the guide field, and $\mathbf{z}^-$ fluctuations propagate parallel to this field. Also, for values of $k_\parallel$ larger than ≈ 20, the dispersion in the excitation of modes increases and energy starts to populate the funnel in spectral space associated with sweeping, indicating random sweeping plays a role at sufficiently small vertical scales. Instead, for $\sigma_c = 0.3$ and 0.9 energy accumulates only near the wave dispersion relation, and we recover counterpropagation of one of the wave motions: both $\mathbf{z}^+$ and $\mathbf{z}^-$ fields propagate in the same direction, antiparallel to the guide field. Increasing B_0 further reduces this effect (see the cases with $B_0 = 8$ in Fig. 6), resulting in the expected propagation for each excitation, or in very little or no propagation of $\mathbf{z}^-$ when σ_c is sufficiently small.

What is the origin of the observed $\mathbf{z}^-$ fluctuations propagating in the same direction as the $\mathbf{z}^+$ fluctuations? Based on the results of Hollweg,[39] and on Eq. (7), they must be caused by reflections in large scale inhomogeneities of the mean magnetic field (note there is no mean background flow in our simulations, nor density fluctuations). Although our background guide field B_0 is uniform (i.e., constant in space as well as in time), the total mean field a fluctuation sees includes a slowly varying component (e.g., from magnetic field fluctuations at large scales, such as those in $k = 1$ modes, which evolve on a slower time scale than fast waves and small-scale fluctuations). As a result, the flow has an effective Alfvén velocity that depends on the spatial coordinates. We can then write for either type of Elsässer fluctuations the ideal linearized Eq. (7) for constant density and for $\mathbf{U} = 0$ (no mean background flow) as

$$\partial_t \mathbf{z}^\pm = \pm \mathbf{V}_A \cdot \nabla \mathbf{z}^\pm \mp \mathbf{z}^\mp \cdot \frac{\nabla \mathbf{B}'}{\sqrt{4\pi\rho}}, \qquad (22)$$

where $\mathbf{V}_A$ can now include large-scale fluctuations of the magnetic field, and $\mathbf{B}'$ as before is the total magnetic field in Gaussian units. If the normalized cross-helicity σ_c is close to 1, that is, if $|\mathbf{z}^+| \gg |\mathbf{z}^-|$, we have for $\mathbf{z}^+$,

$$\partial_t \mathbf{z}^+ \approx \mathbf{V}_A \cdot \nabla \mathbf{z}^+, \qquad (23)$$

and using $\mathbf{z}^\pm = \mathbf{z}_0^\pm e^{i(\mathbf{k}\cdot\mathbf{x} + \omega^\pm t)}$, we recover the usual dispersion relation for waves propagating antiparallel to the mean field $\omega^+ = +\mathbf{V}_A \cdot \mathbf{k}$ (where now $\mathbf{V}_A$ can fluctuate slowly in space and time). However, for $\mathbf{z}^-$, we obtain

$$\partial_t \mathbf{z}^- \approx -\mathbf{V}_A \cdot \nabla \mathbf{z}^- + \mathbf{z}^+ \cdot \frac{\nabla \mathbf{B}'}{\sqrt{4\pi\rho}}. \qquad (24)$$

This equation indicates that the propagation of $\mathbf{z}^-$ perturbations (which are smaller in amplitude than $\mathbf{z}^+$) can be strongly affected by the $\mathbf{z}^+$ field and by spatial variations of the large-scale magnetic field.

From Eq. (24), we can also extract some phenomenological conditions for the behavior seen in Figs. 3–6 (and in particular, for the counterpropagation of waves) to take place. Using again $\mathbf{z}^\pm = \mathbf{z}_0^\pm e^{i(\mathbf{k}\cdot\mathbf{x} + \omega^\pm t)}$, and assuming $\mathbf{B}' = \mathbf{B}_0' + \mathbf{b}_0'$ where $\mathbf{b}_0' = \tilde{\mathbf{b}}_0' e^{i\mathbf{K}\cdot\mathbf{x}}$ is the slowly varying large-scale magnetic field with wavenumber $K \ll k$, Eq. (24) reduces to

$$(\omega^- + \mathbf{V}_A \cdot \mathbf{k})\mathbf{z}_0^- e^{i\omega^- t} = \frac{(\mathbf{K}\cdot\mathbf{z}_0^+)\mathbf{b}_0'}{\sqrt{4\pi\rho}} e^{i\omega^+ t}. \qquad (25)$$

Taking the dot product with $\mathbf{z}_0^-$, defining Elsässer energy densities $e^\pm = |\mathbf{z}_0^\pm|^2/4$, and defining the fluctuations in the Alfvén velocity (associated with the large-scale magnetic field fluctuations) as $\mathbf{v}_A = \mathbf{b}_0'/\sqrt{4\pi\rho}$, we finally get

$$(\omega^- + \mathbf{V}_A \cdot \mathbf{k})e^{i\omega^- t} = \frac{(\mathbf{K}\cdot\mathbf{z}_0^+)(\mathbf{v}_A \cdot \mathbf{z}_0^-)}{4e^-} e^{i\omega^+ t}. \qquad (26)$$

This equation admits solutions

$$\omega^- = \omega^+ = +\mathbf{V}_A \cdot \mathbf{k}, \qquad (27)$$

$$2\mathbf{V}_A \cdot \mathbf{k} = (\mathbf{K}\cdot\mathbf{z}_0^+)(\mathbf{v}_A \cdot \mathbf{z}_0^-)/(4e^-), \qquad (28)$$

which correspond to both waves traveling in the same direction as long as the second condition, given by Eq. (28), can be fulfilled. From dimensional analysis, this condition requires that

$$2\frac{V_A}{v_A}\frac{k}{K} \sim \sqrt{\frac{e^+}{e^-}}, \qquad (29)$$

which (as $V_A \gtrsim v_A$ and $k \gg K$) cannot be satisfied when $\sigma_c \approx 0$ (as observed in Figs. 3–6), or when the guide field becomes too strong for a fixed value of σ_c (as also observed in the spatiotemporal spectra). Thus, this last qualitative argument indicates (in agreement with the simulations) that $\mathbf{z}^-$ fluctuations can propagate with the same phase speed and direction as the $\mathbf{z}^+$ fluctuations as long as $\sigma_c \neq 0$ and B_0 is not too strong for a fixed value of the normalized cross-helicity.

In other words, if $|\mathbf{z}^+|$ at large scales is comparable to $|\mathbf{V}_A|$ and $\sigma_c \approx 1$, we can see $\mathbf{z}^-$ fluctuations propagate in the same direction as $\mathbf{z}^+$ fluctuations as a result of reflections in inhomogeneities of the large-scale magnetic field. A similar behavior can result, for example, from mass density fluctuations when the flow is compressible, as is the case in some regions of the solar wind and the interplanetary medium,[40] and this argument does not preclude other effects such as strong nonlinear interactions from resulting in reflection and counterpropagation of excitations. Moreover, when the intensity of the background magnetic field $\mathbf{B}_0$ is further increased, the arguments used above are not valid anymore and the relevance of the reflections reduces. This is compatible with the behavior seen in Fig. 6 for the

simulations with $B_0 = 8$, which show similar amounts of power in both types of fluctuations when $\sigma_c = 0$, less power in $\mathbf{z}^-$ fluctuations when $\sigma_c = 0.3$ (and propagating opposite to the $\mathbf{z}^+$ field), and no appreciable power for $\mathbf{z}^-$ fluctuations when compared to $\mathbf{z}^+$ in the case with $\sigma_c = 0.9$.
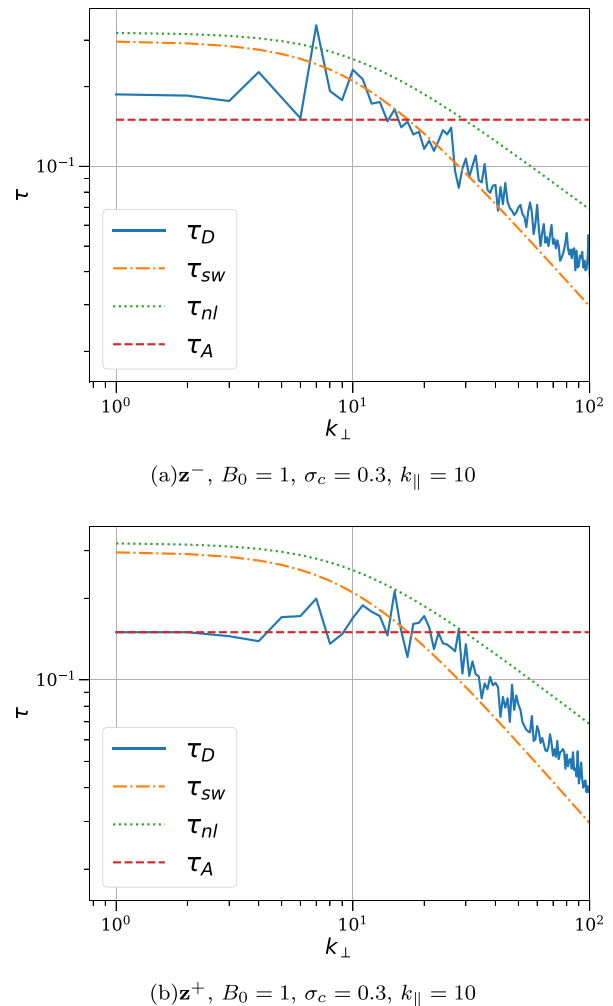
C. Decorrelation times

From the discussions in Sec. II B, another way to identify dominant time scales for individual modes is to study the decorrelation time τ_D, i.e., the time it takes for each Fourier mode with wave vector $\mathbf{k}$ to be decorrelated from its history either by nonlinear eddy interactions (if $\tau_D \sim \tau_{nl}$), by the crossover of waves (if $\tau_D \sim \tau_A$), or by the sweeping by the large-scale flow (when $\tau_D \sim \tau_{sw}$). Again, as τ_D depends on the wave vector $\mathbf{k}$, in the following we show it for fixed values of $k_\parallel$ or $k_\perp$, and as a function of the remaining wavenumber. In all cases, the decorrelation time τ_D is obtained from the numerical data by computing the correlation function $\Gamma(k_\perp, k_\parallel, \tau)$, and looking at the value of the time lag τ for which the correlation function decays to $1/e$ from its value for $\tau = 0$. Note the choice of $1/e$ as a reference value is arbitrary, but similar results are obtained if instead the decorrelation time is defined as the half width of Γ, or as the time when the correlation function crosses the zero.[21,33] With any of these choices, τ_D is a measure of the characteristic time for the decay of the correlation.

Figure 7 shows the different decorrelation times for a fixed value of $k_\parallel = 10$ and as a function of $k_\perp$, for the simulation with $B_0 = 1$ and $\sigma_c = 0.3$. The theoretical predictions for the different decorrelation times are also indicated as a reference. Since the Alfvénic time is independent of $k_\perp$ it shows as a constant vale in this figure. The decorrelation time τ_D obtained from the numerical data is very close to the Alfvénic time for small values of $k_\perp$ (up to $k_\perp \approx 10$), but it deviates and becomes closer to the sweeping time for large values of $k_\perp$ (i.e., for small perpendicular lengthscales). This is more clear for $\mathbf{z}^-$ fluctuations than for $\mathbf{z}^+$ fluctuations, for which the decorrelation time τ_D for $k_\perp > 10$ is in between the scaling of τ_{sw} and of τ_{nl}.

Figure 8 shows the decorrelation times τ_D for the $\mathbf{z}^+$ field for cases with $\sigma_c = 0.3$, with a guide field of $B_0 = 0.25, 1, 4$, and 8, and for fixed $k_\parallel = 15$ as a function of $k_\perp$. Again, for low values of B_0, τ_D is mostly dominated for the sweeping, either for all values of $k_\perp$ (for $B_0 = 0.25$) or down to $k_\perp \approx 20$ (for $B_0 = 1$). However, for larger values of B_0 (or for small values of $k_\perp$ when $B_0 = 1$) Alfvénic effects become dominant, with τ_D taking values close to τ_A. Overall, the fastest time scale at any given $k_\perp$ seems to be the dominant one. These results are consistent with the previous ones we obtained[21] for the case of strong incompressible MHD turbulence with no cross-helicity, although the presence of some cross-helicity in the flow seems to favor a transition toward a flow more dominated by Alfvén waves as also seen in the spatiotemporal spectra in Sec. III B. This can be also associated with the fact that under certain conditions the nonlinear time of the dominant Elsässer fluctuations becomes too long, and the decorrelation time scale is then determined by the so-called "minority species" as reported before in closure calculations by Grappin et al.[41]

This behavior can also be seen when $k_\perp$ is fixed, and τ_D is studied as a function of $k_\parallel$ (see Fig. 9). For simulations with $\sigma_c = 0.3$ and with increasing B_0, we see that τ_D varies with $k_\parallel$ as τ_{sw} when B_0 is small or moderate and when $k_\parallel$ is small, and varies as τ_A when B_0 or $k_\parallel$ are sufficiently large. In other words, modes with wave vectors sufficiently aligned with the guide field are dominated by the Alfvén time. And


(a) $\mathbf{z}^-$, $B_0 = 1$, $\sigma_c = 0.3$, $k_\parallel = 10$

(b) $\mathbf{z}^+$, $B_0 = 1$, $\sigma_c = 0.3$, $k_\parallel = 10$

FIG. 7. Decorrelation times τ_D for the run with $B_0 = 1$ and $\sigma_c = 0.3$, for $k_\parallel = 10$ constant and as a function of $k_\perp$. Panel (a) corresponds to $\mathbf{z}^-$ and panel (b) to $\mathbf{z}^+$. The theoretical prediction for the sweeping time τ_{sw}, the nonlinear time τ_{nl}, and the Alfvén time τ_A are indicated as references.

again, the fastest time scale in this figure is the one that dominates the dynamics.

However, and as mentioned before, this picture changes when σ_c is sufficiently large. This can be seen in Fig. 10, where the decorrelation time τ_D is plotted for the simulations with $B_0 = 1$, for fixed $k_\perp = 40$, and as a function of $k_\parallel$ for $\sigma_c = 0, 0.3$, and 0.9. While for small values of σ_c we observe the same behavior as before, for large values of σ_c the Alfvén time becomes dominant, even when it is slower than all the other time scales, as in the case of the simulation with $\sigma_c = 0.9$ and small values of $k_\parallel$.

Thus, while for small values of σ_c the analysis of the decorrelation time confirms the tendency observed in our previous study[21] that the sweeping time dominates the decorrelations except for the cases with medium and large values of B_0 where the Alfvénic time is dominant for small values of $k_\perp$ or large values of $k_\parallel$ (see also studies of MHD turbulence in the weak regime in Refs. 20 and 42, or of the transition
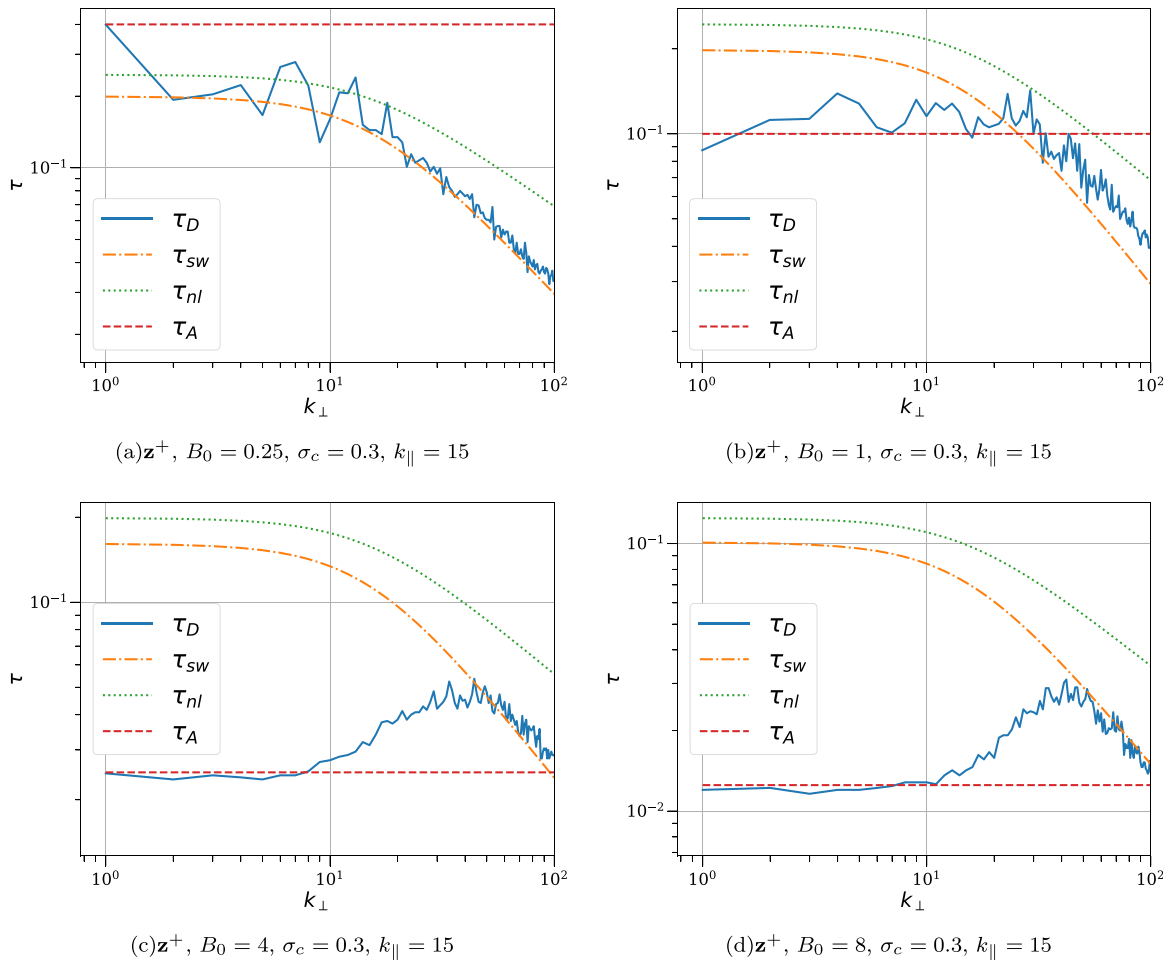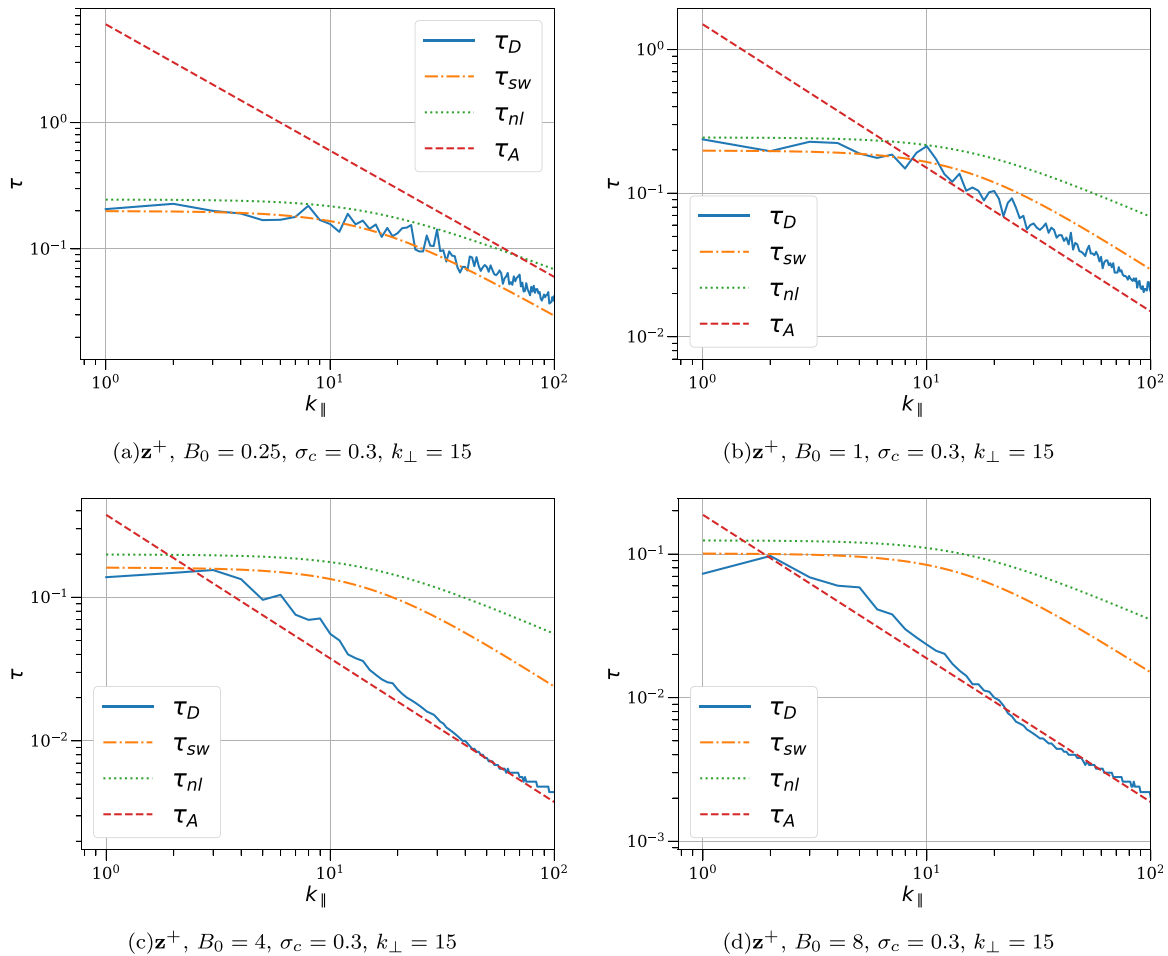
FIG. 8. Decorrelation times τ_D for the $\mathbf{z}^+$ field in simulations with $\sigma_c = 0.3$ and (a) $B_0 = 0.25$, (b) 1, (c) 4, and (d) 8, for $k_{\parallel} = 15$ and as a function of $k_{\perp}$. The theoretical prediction for the sweeping time τ_{sw}, the nonlinear time τ_{nl}, and the Alfvén time τ_A are indicated as references.

from weak to strong MHD turbulence in Refs. 21 and 22) increasing the cross-helicity content of the flow has interesting consequences. The appearance of the Alfvénic time as dominant becomes more clear for large values of σ_c, even when it is not the fastest time scale, and consistent with a linear (or weakly nonlinear) picture in which most of the fluctuations have a single direction of propagation. However, as evidenced in the spatiotemporal analysis of the energy spectrum of each Elsässer field as a function of $\mathbf{k}$ and ω, inhomogeneities of the large scale magnetic field can induce reflections, and turn on nonlinear interactions dominated by the Alfvén crossover time between waves for modes with wave vectors sufficiently aligned with the guide field, or by the sweeping or nonlinear time for other modes.

IV. CONCLUSIONS

We analyzed the spatiotemporal behavior of MHD fluctuations considering their polarizations in terms of the Elsässer variables, using direct numerical simulations of three-dimensional incompressible MHD turbulence. We considered cases with relatively small, intermediate, and large values of a mean background magnetic field and with

null, small, and high cross-helicity. The correlation function as a function of the wavenumber (decomposed in perpendicular and parallel directions to the mean magnetic field) and of the time lag was directly computed for all the different simulations considered, as well as the spatiotemporal spectra. From the correlation functions, we computed the decorrelation time for each Fourier mode, and we compared it with different theoretical predictions for relevant time scales in the system: the local nonlinear time, the random sweeping time, and the Alfvénic time. It was observed that time decorrelations are dominated by sweeping effects for low values of the mean magnetic field and of the cross-helicity, while for large values of the mean magnetic field or of the cross-helicity, time decorrelations are controlled by Alfvénic effects even when the Alfvén time is not the fastest time, a new feature when compared with previous studies of spatiotemporal behavior of strong MHD turbulence with zero cross-helicity. In principle, this behavior could be interpreted as a transition toward a regime with weaker nonlinearities as the cross-helicity is increased, as often argued on theoretical grounds and apparently indicated by our numerical simulations.

FIG. 9. Decorrelation times τ_D for the $\mathbf{z}^+$ field in simulations with $\sigma_c = 0.3$ and (a) $B_0 = 0.25$, (b) 1, (c) 4, and (d) 8, for $k_\perp = 15$ and as a function of $k_\parallel$. The theoretical prediction for the sweeping time τ_{sw}, the nonlinear time τ_{nl}, and the Alfvén time τ_A are indicated as references.

However, it should be noted that the spatiotemporal spectra indicate that even in this regime, nonlinear interactions are relevant: the other main result obtained from our analysis is the finding of a regime in which opposite polarizations $\mathbf{z}^-$ and $\mathbf{z}^+$ fluctuations are generated and propagate in the same direction due to wave reflections caused by inhomogeneities of the large-scale magnetic field. This is more evident in the spatiotemporal spectra of the Elsässer fields for intermediate values of the background magnetic field (that is, when the uniform and constant component of the large-scale magnetic field is not too strong). A phenomenological analysis based on previous ideas in Zhou and Matthaeus[24] confirms the conclusions of Hollweg,[39] which indicate that Alfvénic fluctuations with opposite polarizations can indeed propagate in the same direction and even with the same speed. If the background magnetic field becomes too strong (or if the cross-helicity is close to zero), this effect is no longer observed. Thus, the spatiotemporal analysis of the turbulent flows provides direct evidence of a phenomenon that was predicted before using WKB theory, which can play a relevant role modifying wave propagation and nonlinear interactions in the interplanetary medium.

The results analyzed in this paper show in detail that, at least in the strong turbulence regime, the wave picture is not complete enough to describe the system of incompressible MHD. A broad band of fluctuations appear in this system coming from local and nonlocal (sweeping) effects, which bring in dispersion and nonlinear effects. It is important to recall, of course, that much of the present study has concentrated on the study of the Eulerian decorrelation time, decomposed into a scale-dependent decorrelation time of individual Fourier modes. This decorrelation is generally interpreted as a competition between sweeping decorrelation by large scale fluctuations and decorrelation originating from wave propagation. However, neither of these effects are in principle responsible for the spectral transfer that gives rise to the turbulence cascade. In fact, the main effect of Alfvén propagation, from the perspective of the strong turbulent energy cascade, is not to cause spectral transfer but to suppress it.[43] Understanding the cascade itself requires examination of the strength of the nonlinearities. In this case, the appropriate characteristic time becomes the nonlinear time, whose isolation requires analysis of timescales in the Lagrangian frame[44] (note that only in a few particular cases in our analysis, the
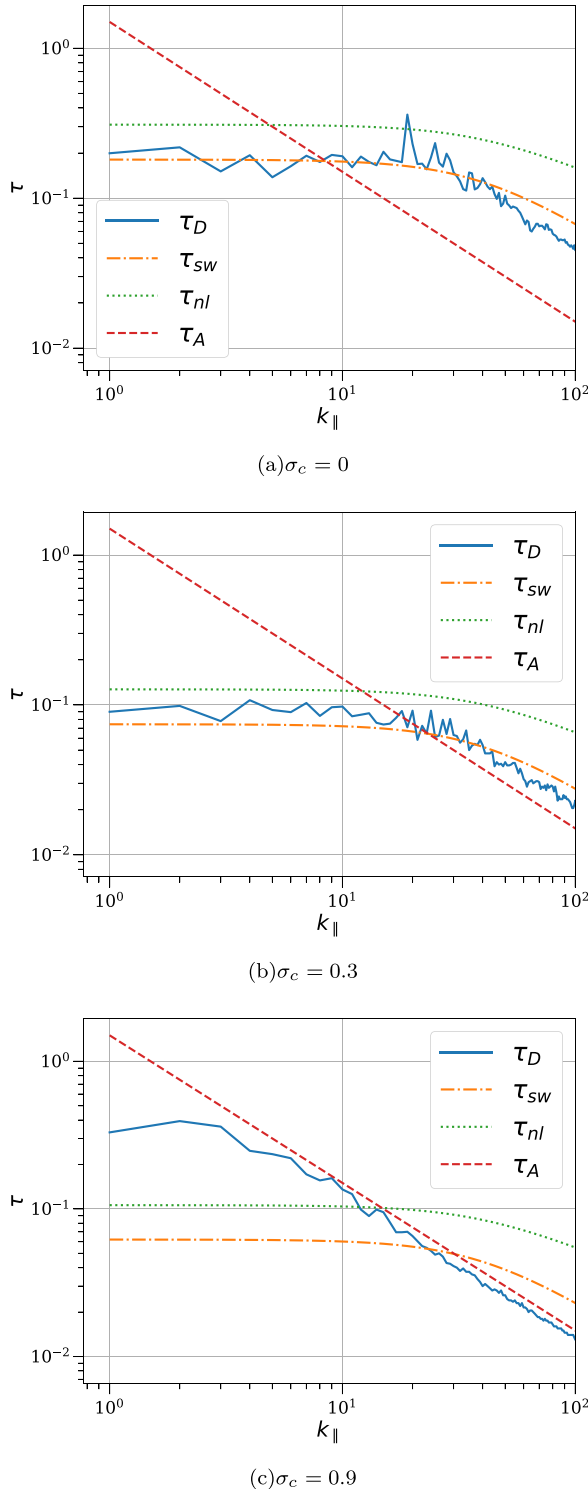
FIG. 10. Decorrelation times τ_D for the runs with $B_0 = 1$, for $k_\perp = 40$ and as a function of $k_\parallel$. The panels correspond to (a) $\sigma_c = 0$, (b) $\sigma_c = 0.3$, and (c) $\sigma_c = 0.9$. The theoretical prediction for the sweeping time τ_{sw}, the nonlinear time τ_{nl}, and the Alfvén time τ_A are indicated as references.

nonlinear time was positively identified as a candidate for the decorrelation time). Nevertheless, we have shown that physically relevant phenomena such as reflection and "anomalous propagation" of reflected fluctuations can produce observable effects in the flow energetics, and these phenomena have been recognized in a variety of configurations of the different controlling parameters of the system, with potential applications.

For example, interesting effects associated with reflection add to the complexity of the dynamics, even in the simplest case of incompressible MHD considered here. This has important implications for applications such as coronal heating, solar wind acceleration, and particle energization in the interplanetary space.[25,26] As a further example, fluctuations observed in the solar wind, which tend to have the magnetic and the velocity field aligned or antialigned (i.e., with different Alfvénic polarizations), cannot always be trivially interpreted as traveling "downstream" or "upstream" the mean magnetic field. Extensions of this study to compressible MHD,[45] considering the dependence with the cross-helicity in the flow and its interplay with compressible effects, as well as a study considering other helicities such as the kinetic helicity H_v or the magnetic helicity H_b and the hybrid helicity for Hall-MHD, would be an interesting follow up of the present study and a first step toward a deeper understanding of the role of nonlinear effects in the propagation of waves in plasma turbulence.

REFERENCES

[1]U. Frisch, *Turbulence: The Legacy of A. N. Kolmogorov* (Cambridge University Press, 1995).

[2]A. Pouquet, U. Frisch, and J. Léorat, "Strong MHD helical turbulence and the nonlinear dynamo effect," J. Fluid Mech. **77**(02), 321–354 (1976).

[3]Y. Zhou, W. H. Matthaeus, and P. Dmitruk, "Magnetohydrodynamic turbulence and time scales in astrophysical and space plasmas," Rev. Mod. Phys. **76**(4), 1015–1035 (2004).

[4]Y. Zhou, A. A. Praskovsky, and G. Vahala, "A non-Gaussian phenomenological model for higher-order spectra in turbulence," Phys. Lett. A **178**(1), 138–142 (1993).

[5]A. Alexakis, P. D. Mininni, and A. Pouquet, "Turbulent cascades, transfer, and scale interactions in magnetohydrodynamics," New J. Phys. **9**(8), 298 (2007).

[6]B. Teaca, M. K. Verma, B. Knaepen, and D. Carati, "Energy transfer in anisotropic magnetohydrodynamic turbulence," Phys. Rev. E **79**(4), 046312 (2009).

[7]H. Aluie and G. L. Eyink, "Scale locality of magnetohydrodynamic turbulence," Phys. Rev. Lett. **104**, 081101 (2010).

[8]P. D. Mininni, "Scale interactions in magnetohydrodynamic turbulence," Annu. Rev. Fluid Mech. **43**(1), 377–397 (2011).

[9]R. H. Kraichnan, "The structure of isotropic turbulence at very high Reynolds numbers," J. Fluid Mech. **5**(04), 497–543 (1959).

[10]H. Tennekes, "Eulerian and Lagrangian time microscales in isotropic turbulence," J. Fluid Mech. **67**(03), 561–567 (1975).

[11]S. Chen and R. Kraichnan, "Sweeping decorrelation in isotropic turbulence," Phys. Fluids A **1**(12), 2019–2024 (1989).

[12]M. Nelkin and M. Tabor, "Time correlations and random sweeping in isotropic turbulence," Phys. Fluids A **2**(1), 81–83 (1990).

[13]W. H. Matthaeus, S. Dasso, J. M. Weygand, M. G. Kivelson, and K. T. Osman, "Eulerian decorrelation of fluctuations in the interplanetary magnetic field," Astrophys. J. **721**(1), L10 (2010).

[14]S. Servidio, V. Carbone, P. Dmitruk, and W. H. Matthaeus, "Time decorrelation in isotropic magnetohydrodynamic turbulence," Europhys. Lett. **96**(5), 55003 (2011).

[15]F. Carbone, L. Sorriso-Valvo, C. Versace, G. Strangi, and R. Bartolino, "Anisotropy of spatiotemporal decorrelation in electrohydrodynamic turbulence," Phys. Rev. Lett. **106**(11), 114502 (2011).

[16]M. Dobrowolny, A. Mangeney, and P. Veltri, "Fully developed anisotropic hydromagnetic turbulence in interplanetary space," Phys. Rev. Lett. **45**(2), 144 (1980).

[17]P. Dmitruk and W. H. Matthaeus, "Waves and turbulence in magnetohydrodynamic direct numerical simulations," Phys. Plasmas **16**(6), 062304 (2009).

[18]A. F. Rappazzo, M. Velli, G. Einaudi, and R. B. Dahlburg, "Coronal heating, weak MHD turbulence, and scaling laws," Astrophys. J. Lett. **657**(1), L47 (2007).

[19]P. Clark di Leoni, P. J. Cobelli, and P. D. Mininni, "The spatio-temporal spectrum of turbulent flows," Eur. Phys. J. E **38**(12), 136 (2015).

[20]R. Meyrand, K. H. Kiyani, and S. Galtier, "Weak magnetohydrodynamic turbulence and intermittency," J. Fluid Mech. **770**, R1 (2015).

[21]R. Lugones, P. Dmitruk, P. D. Mininni, M. Wan, and W. H. Matthaeus, "On the spatio-temporal behavior of magnetohydrodynamic turbulence in a magnetized plasma," Phys. Plasmas **23**(11), 112304 (2016).

[22]R. Meyrand, S. Galtier, and K. H. Kiyani, "Direct evidence of the transition from weak to strong magnetohydrodynamic turbulence," Phys. Rev. Lett. **116**(10), 105002 (2016).

[23]W. H. Matthaeus, Y. Zhou, G. P. Zank, and S. Oughton, "Transport theory and the WKB approximation for interplanetary MHD fluctuations," J. Geophys. Res. **99**(A12), 23421–23430, https://doi.org/10.1029/94JA02326 (1994).

[24]Y. Zhou and W. H. Matthaeus, "Remarks on transport theories of interplanetary fluctuations," J. Geophys. Res. **95**(A9), 14863–14871, https://doi.org/10.1029/JA095iA09p14863 (1990).

[25]M. Velli, "On the propagation of ideal, linear Alfvén waves in radially stratified stellar atmospheres and winds," Astron. Astrophys. **270**, 304–314 (1993).

[26]W. H. Matthaeus, G. P. Zank, S. Oughton, D. J. Mullan, and P. Dmitruk, "Coronal heating by magnetohydrodynamic turbulence driven by reflected low-frequency waves," Astrophys. J. **523**(1), L93–L96 (1999).

[27]P. Dmitruk, W. H. Matthaeus, L. J. Milano, S. Oughton, D. J. Mullan, and G. P. Zank, "Coronal heating distribution due to Alfvenic driven magnetohydrodynamic turbulence," in AGU Spring Meeting Abstracts (2001).

[28]W. H. Matthaeus, S. Oughton, and Y. Zhou, "Anisotropic magnetohydrodynamic spectral transfer in the diffusion approximation," Phys. Rev. E **79**(3), 035401 (2009).

[29]J. Baerenzung, H. Politano, Y. Ponty, and A. Pouquet, "Spectral modeling of turbulent flows and the role of helicity," Phys. Rev. E **77**(4), 046303 (2008).

[30]W. Heisenberg, "Zur statistischen Theorie der Turbulenz," Z. Phys. **124**(7-12), 628–657 (1948).

[31]G. Comte-Bellot and S. Corrsin, "Simple Eulerian time correlation of full-and narrow-band velocity signals in grid-generated, turbulence," J. Fluid Mech. **48**(02), 273–337 (1971).

[32]S. A. Orszag and G. S. Patterson, "Numerical simulation of three-dimensional homogeneous isotropic turbulence," Phys. Rev. Lett. **28**(2), 76–79 (1972).

[33]P. Clark di Leoni, P. J. Cobelli, P. D. Mininni, P. Dmitruk, and W. H. Matthaeus, "Quantification of the strength of inertial waves in a rotating turbulent flow," Phys. Fluids **26**(3), 035106 (2014).

[34]G. K. Batchelor, *The Theory of Homogeneous Turbulence* (Cambridge University Press, 1953).

[35]D. O. Gómez, P. D. Mininni, and P. Dmitruk, "Parallel simulations in turbulent MHD," Phys. Scr. **2005**(T116), 123.

[36]D. O. Gómez, P. D. Mininni, and P. Dmitruk, "MHD simulations and astrophysical applications," Adv. Space Res. **35**(5), 899–907 (2005).

[37]P. D. Mininni, D. Rosenberg, R. Reddy, and A. Pouquet, "A hybrid MPI-OpenMP scheme for scalable parallel pseudospectral computations for fluid turbulence," Parallel Comput. **37**, 316–326 (2011).

[38]P. D. Mininni, D. Rosenberg, and A. Pouquet, "Isotropization at small scales of rotating helically driven turbulence," J. Fluid Mech. **699**, 263–279 (2012).

[39]J. V. Hollweg, "On WKB expansions for Alfvén waves in the solar wind," J. Geophys. Res. **95**(A9), 14873–14879, https://doi.org/10.1029/JA095iA09p14873 (1990).

[40]Y. Zhou and W. H. Matthaeus, "Non-WKB evolution of solar wind fluctuations: A turbulence modeling approach," Geophys. Res. Lett. **16**(7), 755–758, https://doi.org/10.1029/GL016i007p00755 (1989).

[41]R. Grappin, J. Leorat, and A. Pouquet, "Dependence of MHD turbulence spectra on the velocity field-magnetic field correlation," Astron. Astrophys. **126**, 51–58 (1983).

[42]S. Galtier, S. V. Nazarenko, A. C. Newell, and A. Pouquet, "A weak turbulence theory for incompressible magnetohydrodynamics," J. Plasma Phys. **63**(5), 447–488 (2000).

[43]J. V. Shebalin, W. H. Matthaeus, and D. Montgomery, "Anisotropy in MHD turbulence due to a mean magnetic field," J. Plasma Phys. **29**(3), 525–547 (1983).

[44]R. H. Kraichnan, "Kolmogorov's hypotheses and Eulerian turbulence theory," Phys. Fluids **7**(11), 1723–1734 (1964).

[45]N. Andrés, P. Clark Di Leoni, P. D. Mininni, P. Dmitruk, F. Sahraoui, and W. H. Matthaeus, "Interplay between Alfvén and magnetosonic waves in compressible magnetohydrodynamics turbulence," Phys. Plasmas **24**(10), 102314 (2017).